

# Measurement of the Spectrum of UHE Cosmic Rays by the FADC Detector of the HiRes Experiment

T. Abu-Zayyad<sup>a</sup> G.C. Archbold<sup>a</sup> J.A. Bellido<sup>b</sup> K. Belov<sup>a</sup>  
 J.W. Belz<sup>c</sup> D.R. Bergman<sup>d,1</sup> J. Boyer<sup>e</sup> Z. Cao<sup>a</sup> R.W. Clay<sup>b</sup>  
 B.R. Dawson<sup>b</sup> A.A. Everett<sup>a</sup> J.H.V. Girard<sup>a</sup> R.C. Gray<sup>a</sup>  
 W.F. Hanlon<sup>d</sup> B.F. Jones<sup>a</sup> C.C.H. Jui<sup>a</sup> D.B. Kieda<sup>a</sup> K. Kim<sup>a</sup>  
 B. Knapp<sup>e</sup> E.C. Loh<sup>a</sup> K. Martens<sup>a</sup> G. Martin<sup>f</sup> N. Manago<sup>g</sup>  
 E.J. Mannel<sup>e</sup> J.A.J. Matthews<sup>f</sup> J.N. Matthews<sup>a</sup> J.R. Meyer<sup>a</sup>  
 S.A. Moore<sup>a</sup> P. Morrison<sup>a</sup> A.N. Moosman<sup>a</sup> J.R. Mumford<sup>a</sup>  
 M.W. Munro<sup>c</sup> L. Perera<sup>d</sup> K. Reil<sup>a</sup> R. Riehle<sup>a</sup> M. Roberts<sup>f</sup>  
 M. Seman<sup>e</sup> M.A. Schindel<sup>c</sup> S. Schnetzer<sup>d</sup> P. Shen<sup>a</sup>  
 K.M. Simpson<sup>b</sup> J.D. Smith<sup>a</sup> P. Sokolsky<sup>a</sup> C. Song<sup>e</sup>  
 R.W. Springer<sup>a</sup> B.T. Stokes<sup>a</sup> S.B. Thomas<sup>a</sup> G.B. Thomson<sup>d</sup>  
 S. Westerhoff<sup>e</sup> L.R. Wiencke<sup>a</sup> T.D. VanderVeen<sup>a</sup> A. Zech<sup>d</sup>  
 X. Zhang<sup>e</sup>

<sup>a</sup>*University of Utah, Department of Physics and High Energy Astrophysics  
Institute, Salt Lake City, Utah, USA*

<sup>b</sup>*University of Adelaide, Department of Physics, Adelaide, South Australia,  
Australia*

<sup>c</sup>*University of Montana, Department of Physics and Astronomy, Missoula,  
Montana, USA*

<sup>d</sup>*Rutgers - The State University of New Jersey, Department of Physics and  
Astronomy, Piscataway, New Jersey, USA*

<sup>e</sup>*Columbia University, Department of Physics and Nevis Laboratory, New York,  
New York, USA*

<sup>f</sup>*University of New Mexico, Department of Physics and Astronomy, Albuquerque,  
New Mexico, USA*

<sup>g</sup>*University of Tokyo, Institute for Cosmic Ray Research, Kashiwa, Japan*

The High Resolution Fly's Eye Collaboration

---

**Abstract**

We have measured the spectrum of UHE cosmic rays using the flash ADC (FADC) detector (called HiRes-II) of the High Resolution Fly's Eye experiment running in monocular mode. We describe in detail the data analysis, development of the Monte Carlo simulation program, and results. We also describe the results of our other detector, HiRes-I. We present our measured spectra and compare them with a model incorporating galactic and extragalactic cosmic rays.

---

## 1 Introduction

The aim of the High Resolution Fly's Eye experiment (HiRes) is to study the highest energy cosmic rays using the atmospheric fluorescence technique. In this paper we describe the data collection, analysis, and Monte Carlo calculations used to measure the cosmic ray spectrum with the HiRes experiment's FADC detector, HiRes-II. We also describe the analysis performed on the data collected by the HiRes-I detector and present the two monocular spectra, covering an energy range from  $2 \times 10^{17}$  eV to over  $10^{20}$  eV. We describe a fit of our data to a model incorporating galactic and extragalactic cosmic ray sources.

At these energies the acceleration of cosmic rays is thought to occur in large regions of high magnetic fields expanding at relativistic velocities [1]. Regions such as these are rare in the neighborhood of the Milky Way galaxy and many of the cosmic rays that we observe may have traveled cosmological distances to reach us. Hence they are probes of conditions in some of the most violent and interesting objects in the universe.

The highest energy particles from man-made accelerators have energy  $1 \times 10^{12}$  eV so the cosmic rays we observe have energies at least five orders of magnitude higher. Since we observe showers in the atmosphere initiated by the cosmic ray particles we are sensitive to their composition and to the details of their interactions with matter. New physics with threshold above current accelerator energies may be observable by studying the highest energy cosmic rays.

Interactions of high energy protons, traveling large distances across the universe, with photons of the cosmic microwave background radiation can excite nucleon resonances which decay to a nucleon plus a  $\pi$  meson. This is an important energy loss mechanism for the cosmic rays, which results in the Greisen-Zatsepin-Kuzmin (GZK) cutoff [2], which is often stated as: cosmic rays traveling more than 50 Mpc should have a maximum energy of  $6 \times 10^{19}$

---

<sup>1</sup> To whom correspondence should be addressed. E-mail: dbergman@physics.rutgers.edu

eV, if sources are uniformly distributed. Several events above this energy have been seen by previous experiments [3,4,8], but statistics are low and it is crucial to search for more events above the GZK cutoff.

The spectrum of cosmic rays has few distinguishing features. It consists of regions of power law behavior with breaks in the power law index. There is a steepening from  $E^{-2.7}$  to  $E^{-3.0}$  at about  $3 \times 10^{15}$  eV (called the knee) [9] and a hardening at higher energy (called the ankle). The Fly's Eye experiment [4], observing in stereo mode, saw a second knee (or steepening of the spectrum) at  $4 \times 10^{17}$  eV and the ankle at  $3 \times 10^{18}$  eV. The second knee has also been observed by the Akeno experiment [5]. The Haverah Park experiment [6] observed the ankle at about  $4 \times 10^{18}$  eV. The Yakutsk experiment [7] has seen both the second knee and the ankle. The AGASA experiment [8], which is large enough to reach  $10^{20}$  eV, observes a higher flux, the ankle at  $1 \times 10^{19}$  eV, and no hint of the GZK cutoff.

The atmospheric fluorescence technique has its basis in the fact that on average five UV fluorescence photons will be emitted when a minimum ionizing particle of charge  $e$  passes through one meter of air at standard temperature and pressure. In HiRes we detect these photons and reconstruct the development of cosmic ray air showers. We collect the fluorescence light with spherical mirrors of area  $5.1 \text{ m}^2$ , and focus it on a  $16 \times 16$  array of photomultiplier tubes, each of which looks at about 1 square degree of the sky. We save pulse height and time of arrival information from each tube, and can reconstruct the geometry of the air shower and the energy of the primary cosmic ray that initiated it.

HiRes consists of two detectors located atop desert hilltops on the U. S. Army Dugway Proving Ground in west central Utah. One detector, called HiRes-I, consists of 22 mirrors that look between 3 and 17 degrees in elevation and almost 360 degrees in azimuthal angle [10]. This detector uses a sample-and-hold readout system to save the photomultiplier tubes' pulse height and time information.

The second detector, called HiRes-II, is located 12.6 km away, consists of 42 mirrors, covers between 3 and 31 degrees in elevation, and has a flash ADC (FADC) system to save pulse height and time information from its phototubes [11]. The sampling period of the FADC electronics is 100 ns. The HiRes detectors can trigger on and reconstruct cosmic ray air showers that occur within a radius of about 35 km.

The two detectors are designed to observe cosmic ray showers stereoscopically. This stereo mode observation gives us the best geometric resolution, about 0.3 degrees in pointing angle and 100 m in distance to the shower. In stereo mode we make two measurements of the particle's energy and thus can measure our

energy resolution. The only drawback of stereo mode is that the events of lowest observable energy lie halfway between the two detectors, about 6 km from each detector, and must have energy greater than about  $10^{18}$  eV.

In monocular observation, the HiRes-II detector can see events much closer and hence dimmer and of lower energy: about  $2 \times 10^{17}$  eV is the lower limit. The geometric resolution is still good: about 5 degrees in pointing angle and 300 m in distance. In this paper we describe the operation and data analysis for the HiRes-II detector, briefly describe the differences between HiRes-I and HiRes-II, and present the monocular spectra of the two detectors.

## 2 Calibration Issues

There are two important calibration issues in HiRes: the first is the absolute calibration of the phototubes' pulse heights in photons. This is accomplished by carrying a standard light source to each of our detectors and illuminating the phototubes with it [12]. This source is calibrated to about 10% accuracy and this uncertainty appears in our energy measurements.

Since the atmosphere is both our calorimeter and the medium through which we look, we must correct for the way it absorbs and scatters fluorescence light. The determination of the characteristics of the atmosphere is our second important calibration. Both the molecular and aerosol components of the atmosphere contribute to the scattering. The molecular component is well known, but we must measure the aerosol component's contribution. This calibration is performed by firing an UV laser from one of our detector sites, allowing the atmosphere to scatter the laser light, and observing the scattered light with our other detector. In this way we measure the scattering length, angular distribution of the scattering cross section, and vertical aerosol optical depth (VAOD) of aerosol particles in the atmosphere [13]. The aerosol scale height is obtained from the product of Horizontal scattering length at ground level times the VAOD.

Figure 1 shows the amount of light detected as a function of scattering angle for one of these laser shots. This shot was fired horizontally from the HiRes-II site and passed within 400 meters of the HiRes-I detector. This geometry allows us to observe a wide range of scattering angles. The black points show the data, and the open points are a fit to this data using a four parameter model of the aerosol scattering length and angular distribution. The forward peak seen in this figure is characteristic of aerosol scattering and the relatively flat distribution at backward scattering angles is characteristic of molecular scattering. The aerosol horizontal scattering length measured from these data is 23 km. For comparison, the molecular scattering length at 355 nm is 18 km.

These scattering lengths correspond approximately to the average of atmospheric conditions.

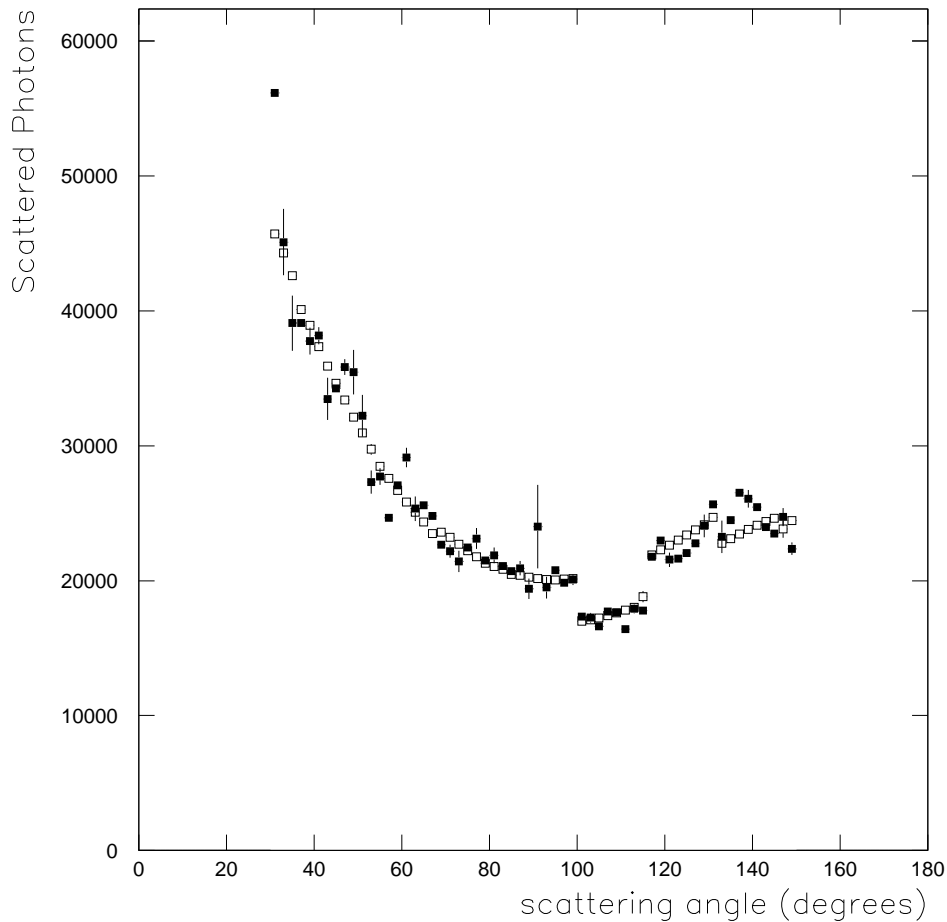


Fig. 1. Intensity of laser light scattered into the HiRes-I detector plotted against the scattering angle of the light. The black points are the data and the open points are a four-parameter fit to the data. The discontinuity between 100 and 116 degrees is due to parallax of a mirror farther from the laser track.

We perform the laser measurement of atmospheric conditions hourly during data collection. For the analysis reported here the average of hourly aerosol scattering lengths and scale heights were used. Since the data has good statistics and the events were collected evenly over the period in question, they will be well described by the average atmospheric conditions [13], which were: aerosol scattering length of  $22 \pm 2$  km and scale height of 1.1 km. The RMS of the scale height distribution was 0.4 km, and the systematic uncertainty was smaller than this.

### 3 Data Analysis

The FADC data acquisition system records a  $10 \mu\text{s}$  long series of ADC samples (100 samples total) for each active photomultiplier tube (PMT) in an event. The starting time of the series is chosen to have the peak of the signal pulse in the middle of the sample.

The first step in the analysis of the data consists of pattern recognition to choose which hit tubes were on the track of the cosmic ray event. As a cosmic ray shower propagates down through the atmosphere the mirrors collect its fluorescence photons and focus them onto the array of phototubes. The image moves across the array illuminating one or more tubes at a time. Therefore, tubes on the cosmic ray track are near each other in two ways: spatially and temporally. Phototubes must be near each other in both position and time to be included in the track. The top two quarters of Figure 2 show the picture of an event, where one can see that the tubes on the shower form a line. The lower left part of this figure is a time plot: a plot of the light arrival times (in FADC time-bin units) on the vertical axis versus the angle of the tube measured along the track. From these plots it is clear which tubes are part of the track. The elevation and azimuthal angles of the PMT's on the track are fit to determine the plane which contains the shower and the detector.

In a monocular determination of the shower geometry, the angle of the shower within the shower detector plane is determined from the time plot of the active tubes (see the lower left quadrant of Figure 2). One can show that

$$t_i = t_0 + \frac{R_p}{c} \tan\left(\frac{\pi - \psi - \theta_i}{2}\right) \quad (1)$$

where  $t_i$  is the arrival time of light from shower segment  $i$ ,  $\theta_i$  is the angle in the plane containing the shower and detector from the ground to segment  $i$ ,  $t_0$  is the earliest possible arrival time,  $R_p$  is the impact parameter of the shower, and  $\psi$  is the angle the shower makes with the ground in the shower-detector plane. We measure  $t_i$  and  $\theta_i$ , and need to fit for  $t_0$ ,  $\psi$  and  $R_p$ .  $\psi$  and  $R_p$  determine the geometry within the shower-detector plane. Since equation 1 is linear in  $R_p$  and  $t_0$ , we fit for those variables for fixed  $\psi$ , for  $5^\circ \leq \psi \leq 175^\circ$  in  $1^\circ$  steps. The best geometry is chosen by minimizing  $\chi^2$ , and the uncertainty in  $\psi$  from the angles which increase the  $\chi^2$  by one.

Once the geometry of the shower is known we can reconstruct the number of charged particles in the shower as a function of the slant depth of atmosphere through which the shower passed. To do this we collect the photoelectrons from tubes on the track into successive time bins. Typically several tubes will contribute to each time bin. We then correct for the sum of the acceptance of

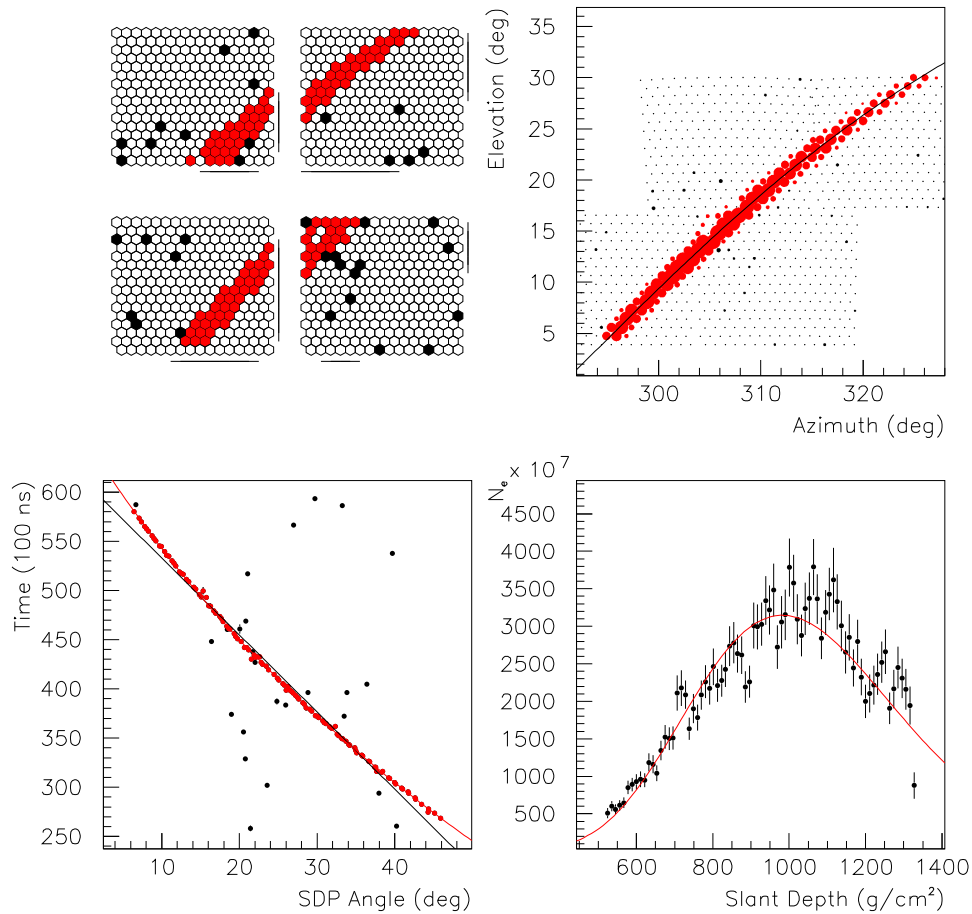


Fig. 2. Display of an Event with a Reconstructed Energy of 52 EeV. The upper left part of this figure shows the four mirrors that triggered for this event. The upper right panel shows the azimuthal vs. elevation angles of triggered tubes, with a fit superimposed. The lower left panel shows the time of the tube hits in FADC time slices vs. the angle of the tube measured along the track, with two fits superimposed: a straight line and the result of the time fit. The lower right quarter shows the number of charged particles in the shower as a function of slant depth (in  $\text{g}/\text{cm}^2$ ), with the fit to the Gaisser-Hillas formula superimposed.

all the participating PMT's and for the quantum efficiency of the phototubes. This photon count is converted into a number of charged particles at the observed position of the shower using the mirror area, distance to the shower, and fluorescence yield. It also includes a loss factor due to the attenuation in the atmosphere. The lower right part of Figure 2 shows the development profile of a shower.

The charged particle multiplicity distribution is fit to the Gaisser-Hillas profile

function [14]:

$$N(x) = N_{max} \left( \frac{x - x_0}{x_{max} - x_0} \right)^{\frac{x_{max} - x_0}{\lambda}} \exp\left( \frac{x_{max} - x}{\lambda} \right), \quad (2)$$

where  $N(x)$  is the number of charged particles in the shower at slant depth  $x$ ,  $N_{max}$  is the number of particles at shower maximum,  $x_{max}$  is the slant depth of the maximum, and  $\lambda$  is a shower-development parameter. We have seen in previous measurements that the Gaisser-Hillas profile function fits our data very well [15]. Our fits are very insensitive to  $x_0$  and  $\lambda$  and we fix them at -60 and 70 g/cm<sup>2</sup>, respectively. The  $x_0$  value is chosen to agree with our fits to Corsika showers (see below). We integrate the Gaisser-Hillas function over  $x$  and multiply by the average energy loss per particle (2.19 MeV/g/cm<sup>2</sup>) to determine the visible shower energy. The visible energy is then corrected for energy carried off by unobservable particles [17] to give the total shower energy.

The charged particles of the shower are accompanied by a large flux of Cerenkov photons, and some of these photons are scattered by the molecular and aerosol components of the air into the acceptance of our experiment. We correct for this effect by using the Gaisser-Hillas fit to predict the flux of Cerenkov photons. This light is subtracted from the signal used to determine the shower development profile, and the process is iterated until the shower development profile plus the calculated scattered Cerenkov light agrees with our measurement. This correction is typically about 15%.

The cuts that are applied to the data to select events which have good resolution and can be used for the determination of the UHE cosmic ray spectrum are listed below.

- Angular speed  $< 11^\circ \mu s^{-1}$
- Selected tubes  $\geq 7$
- $0.85 < \text{Tubes/degree} < 3.0$
- Photoelectrons/degree  $> 25$
- Track length  $> 7^\circ$ , or  $> 10^\circ$  for events extending above  $17^\circ$  elevation
- Zenith angle  $< 60^\circ$
- $150 < X_{max} < 1200 \text{g/cm}^2$ , and is visible in detector
- Average Cerenkov Correction  $< 60\%$
- Geometry fit  $\chi^2/\text{d.o.f.} < 10$
- Profile fit  $\chi^2/\text{d.o.f.} < 10$



## 4 Development of the Monte Carlo Simulation Program

We calculated the aperture of the detector using two Monte Carlo simulation programs. First we generated a library of cosmic ray showers using the programs CORSIKA [18] and QGSJET [19]. We then use events from the library as input to a second program which calculates the response of the detector and writes out simulated events in the same format as the data. Finally, we analyze the Monte Carlo events using the same programs used for the data.

The shower library consists of 200 showers with proton and 200 showers with iron primaries generated for each combination of five fixed primary energies from  $10^{16}$  eV to  $10^{20}$  eV and three fixed zenith angles of the shower axis with a secant of 1.00, 1.25 and 1.50. Each shower is characterized by its depth of first interaction in the atmosphere, energy, zenith angle, type of primary particle, and the four parameters of a Gaisser-Hillas fit to its profile (the Gaisser-Hillas formula fits CORSIKA + QGSJET showers very well).

When we use these events we must scale their parameters in energy from the (discrete) energies of the shower library to the continuous energy spectrum we throw in the detector-response Monte Carlo program. Figure 3 shows the energy dependence of the four Gaisser-Hillas parameters. In scaling the parameters of a shower we use the slopes shown in the four parts of this figure. Use of a shower library preserves the event-to-event fluctuations and correlations in the CORSIKA events.

Since we change the geometry of the showers at random, one CORSIKA shower can be used over and over to create different events. This allow us to generate approximately 30 times as many events per minute with the shower library as we could directly with CORSIKA.

The detector-response program simulates the operation of the two HiRes detectors, including optics, trigger, electronics, and data acquisition. To generate an event, the program chooses the primary energy and the primary particle type from the spectrum and composition measured by the Fly's Eye experiment [4]. The zenith angle and distance to the shower are chosen randomly. An event from the shower library bin whose fixed energy and zenith angle are closest to the chosen values is then used to generate the profile of the shower's development. We scale each of the four Gaisser-Hillas parameters to the thrown energy. The dependence of the Gaisser-Hillas parameters on zenith angle is quite weak, hence we simply use the three bins in zenith angle.

To simulate the exact conditions of the experiment, we created a database of parameters that vary from night to night: live time, trigger logic, trigger gains and thresholds, and number of mirrors in operation. Two parameters which vary with time, but which we treated only in an average way, are the sky noise

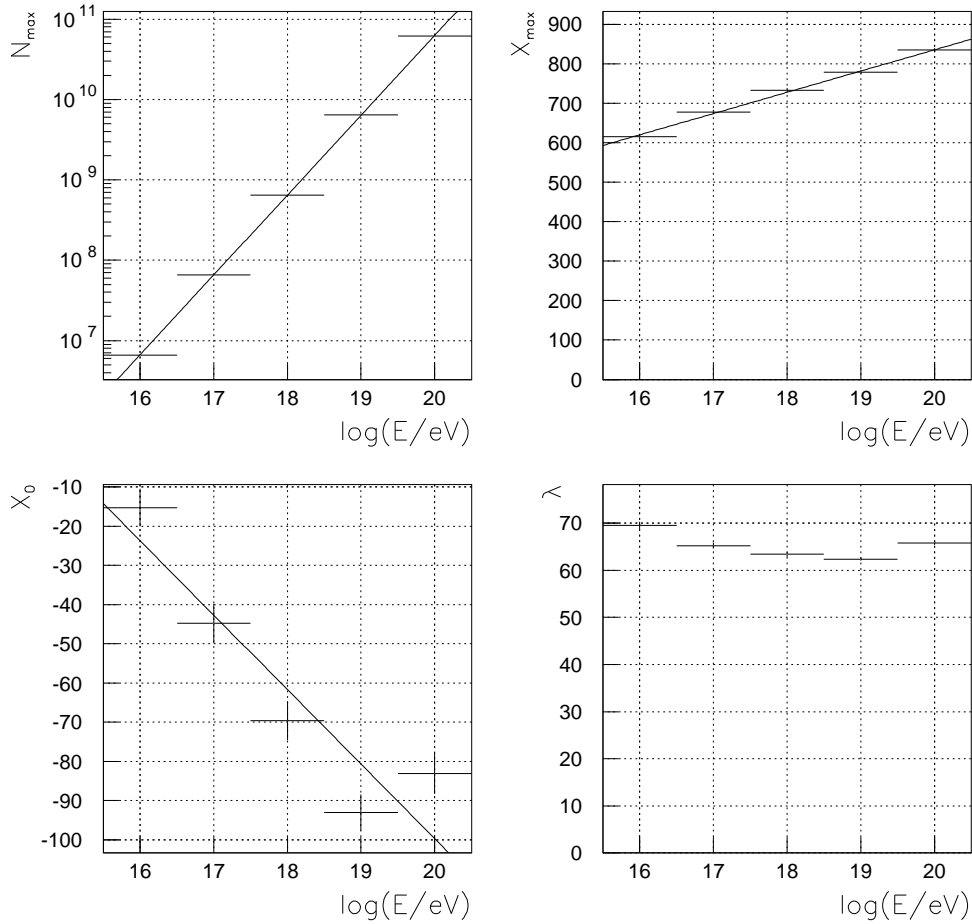


Fig. 3. Energy Dependence of Gaisser-Hillas Parameters. The four panels show (clockwise from upper left) the energy dependence of  $N_{max}$ ,  $x_{max}$ ,  $\lambda$ , and  $x_0$  for showers at zenith angle of 36.9 degrees.

and atmospheric scattering of fluorescence light.

These parameters are read into the detector response programs event by event, allowing us to simulate events with the values of these parameters exactly as happened in the data. Direct comparisons of Monte Carlo events and real data, such as those shown below, give us confidence in our detector response programs and prove that we understand our detectors.

The data that went into the comparison plots shown below were recorded by the HiRes-II-detector from 1 December 1999, through 4 May 2000. There are about 2100 events after cuts. The Monte Carlo sample contains about five times as many events. The first two graphs presented here show two basic geometric quantities: the zenith angle distribution and the distance to the

shower mean (found by weighting each PMT that was on the track by the number of observed photoelectrons). The upper panels of the graphs show the data as filled squares and the Monte Carlo as open squares. The data and MC distributions have been normalized to cover the same area. In the lower panels, the ratio of data divided by MC and a linear fit to this ratio are shown. It can be seen from Figures 4 and 5 that the distributions of these geometric quantities agree very well. Figure 6 shows the  $\chi^2$  of a linear fit to the time plot (such as is shown in the lower left quadrant of Figure 2). The agreement shows that the experimental resolution is well simulated in the Monte Carlo program. An important non-geometric quantity is the amount of light that is seen by the detector. It can be characterized by the number of photoelectrons we receive per degree of track. Figure 7 shows that the amount of light we see with our detectors and the amount of light we generate in our MC programs closely agree with each other. Figure 8 shows a histogram of the reconstructed energy of events.

The excellent agreement between the data and Monte Carlo simulation in these plots is characteristic of our Monte Carlo as a whole.

## 5 The UHE Cosmic Ray Spectrum

Having demonstrated that our MC models the detector accurately, we have confidence in using it to calculate the detector aperture. This aperture is shown in Figure 9.

To make an accurate calculation of the flux of cosmic rays it is important to use a continuous Monte Carlo input spectrum in order to take account of the finite energy resolution of the detector. With this in mind, we define the flux,  $J(E)$ , as follows:

$$J(E) = N_D(E) \frac{N_T(E)}{N_A(E)} \frac{1}{\Delta E A \Omega T} \quad (3)$$

where  $N_D(E)$  is the number of data events in energy bin  $E$ ,  $N_T(E)$  is the number of thrown MC events in energy bin  $E$  binned by the thrown energy,  $N_A(E)$  is the number of accepted MC events in energy bin  $E$  binned by the reconstructed energy,  $\Delta E$  is the width of energy bin  $E$ ,  $A$  is the area into which the MC generated events,  $\Omega$  is the solid angle into which the MC generated events, and  $T$  is the total running time of the detector. The MC generated events within a 30 km radius of the detector and with zenith angles from  $0^\circ$  to  $70^\circ$ . For the data included in this paper, recorded from 1 December 1999 to 4 May 2000, the detector was live for 519400 s (144:16:40). This includes data only from nights with good weather.

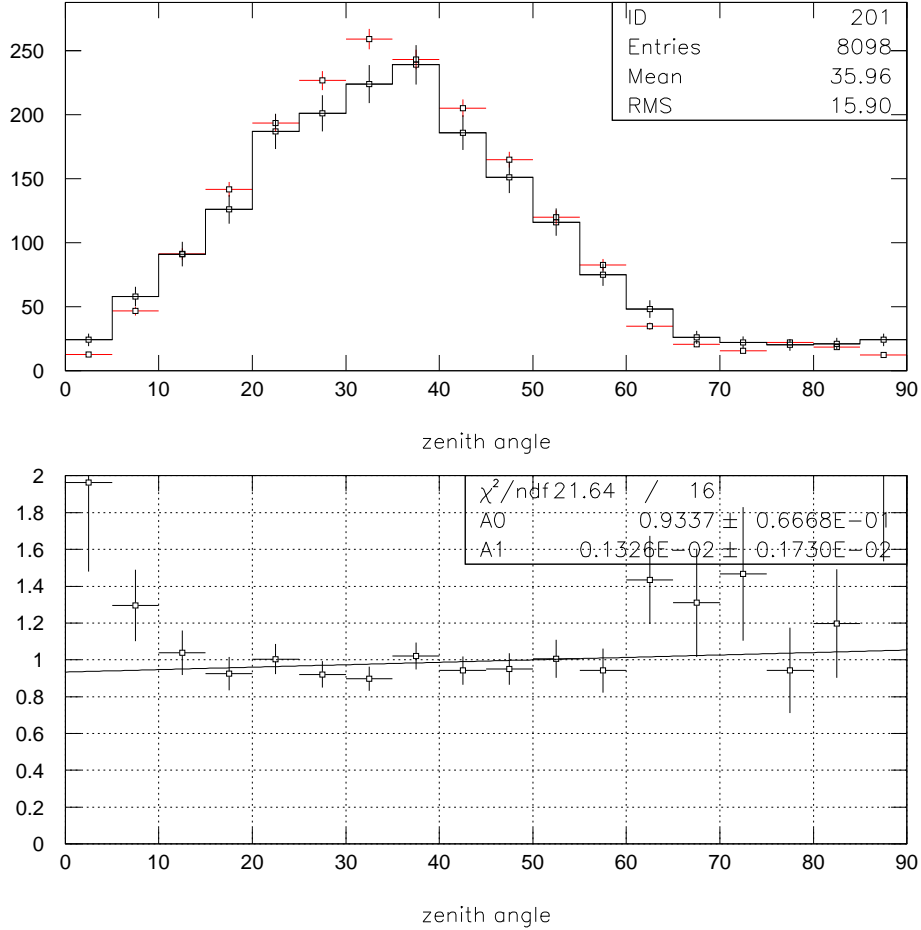


Fig. 4. Zenith Angle of Cosmic Ray Showers. In the upper panel the data is shown as solid black squares and the Monte Carlo (which has been normalized to the number of data events) is shown as open squares. The lower panel shows the ratio of data to Monte Carlo events.

An important feature of Equation 3 is that when one has modeled the experimental resolution correctly and put in the correct thrown energy spectrum,  $N_T(E)$ , the ratio  $N_D(E)/N_A(E)$  becomes a constant independent of energy. In this situation one has corrected for experimental resolution: the spectrum one calculates has the shape of  $N_T(E)$ . The comparisons between data and Monte Carlo (see especially Figures 6 and 8) show that our modeling is accurate.

The measured spectrum,  $J(E)$ , is shown in Figure 10. The measured spectrum multiplied by  $E^3$  is shown in Figure 11. For the latter, the average energy of the data events in each bin is used to compute the  $E^3$  factor.

The agreement with the Fly’s Eye stereo spectrum [4] (also shown in Figure 11) is good. The HiRes-II results are consistently lower than that of the Fly’s Eye

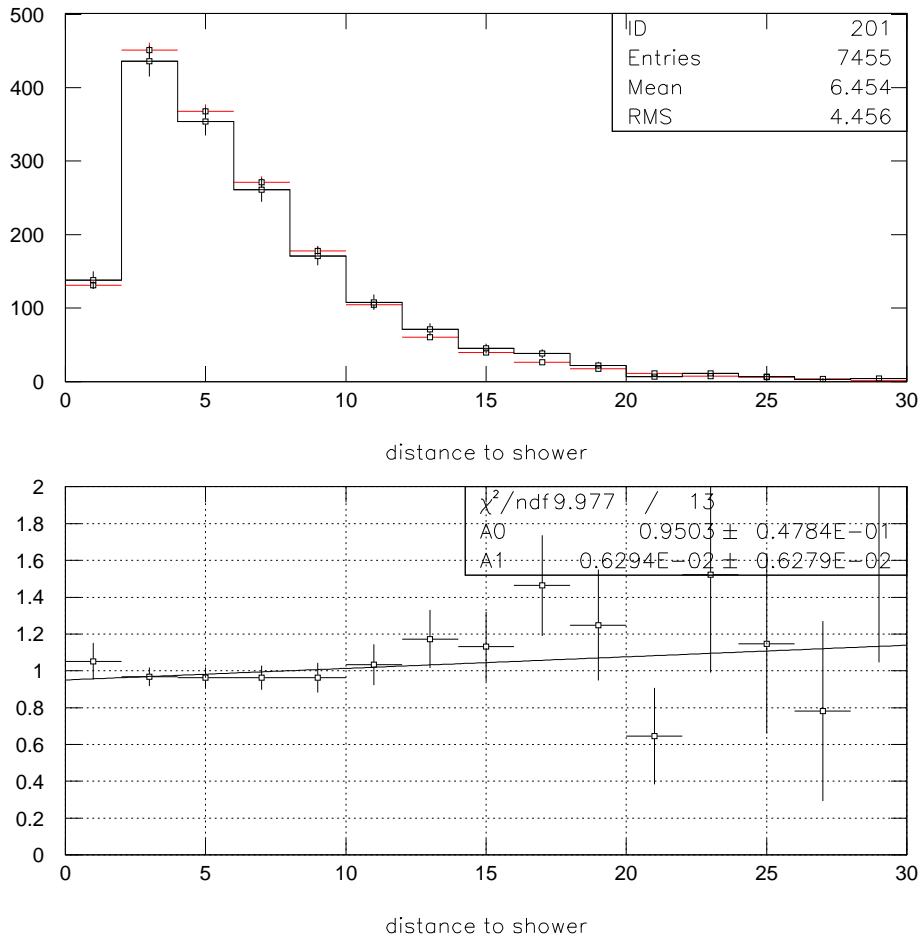


Fig. 5. Distance from the Detector to the Shower Mean (weighted by photoelectrons). Again data is shown in black and Monte Carlo in red, and the lower panel shows the data to Monte Carlo ratio.

experiment, but are within the normalization uncertainty of each experiment.

## 6 Systematic Uncertainties

The largest sources of systematic uncertainty in this experiment are atmospheric modeling, the absolute calibration of the detector in units of photons, the absolute yield of the fluorescence process, and the correction for unobserved energy in the shower.

To test the sensitivity of the flux measurement to uncertainties in atmospheric conditions we reanalyzed the data and generated new Monte Carlo samples

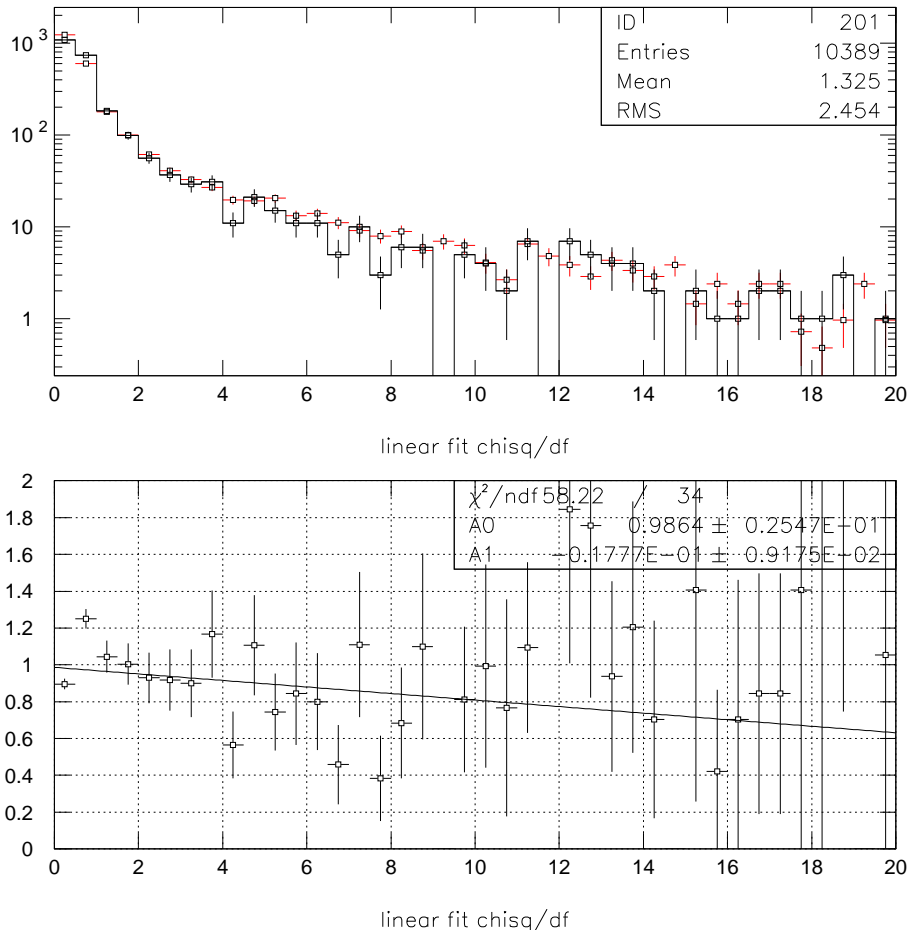


Fig. 6. Chi-squared of a linear fit to the time vs angle plot.

with new conditions: we first changed the aerosol horizontal extinction length from 22 to 20 km, then we changed the aerosol scale height from 1.1 km to 0.7 km. The extinction length change corresponds to one standard deviation. For the scale height change we used the RMS of the scale height distribution, and thus made a conservative estimate of the systematic uncertainty from this source. These two variables are related since the aerosol column depth is equal to their product (for an exponential atmospheric model). Changing the horizontal extinction length had little effect, raising the normalization of  $J(E)$  by  $(4 \pm 6)\%$ . The change in aerosol scale height had a larger effect, lowering  $J(E)$  on average by  $(15 \pm 5)\%$ . We also raised the scale height and found a symmetric change in  $J(E)$ .

The systematic uncertainty from the absolute calibration of the detector is equal to 10% and is independent of energy [12]. The absolute uncertainty in the fluorescence yield is 10% and is independent of energy [16]. The uncertainty

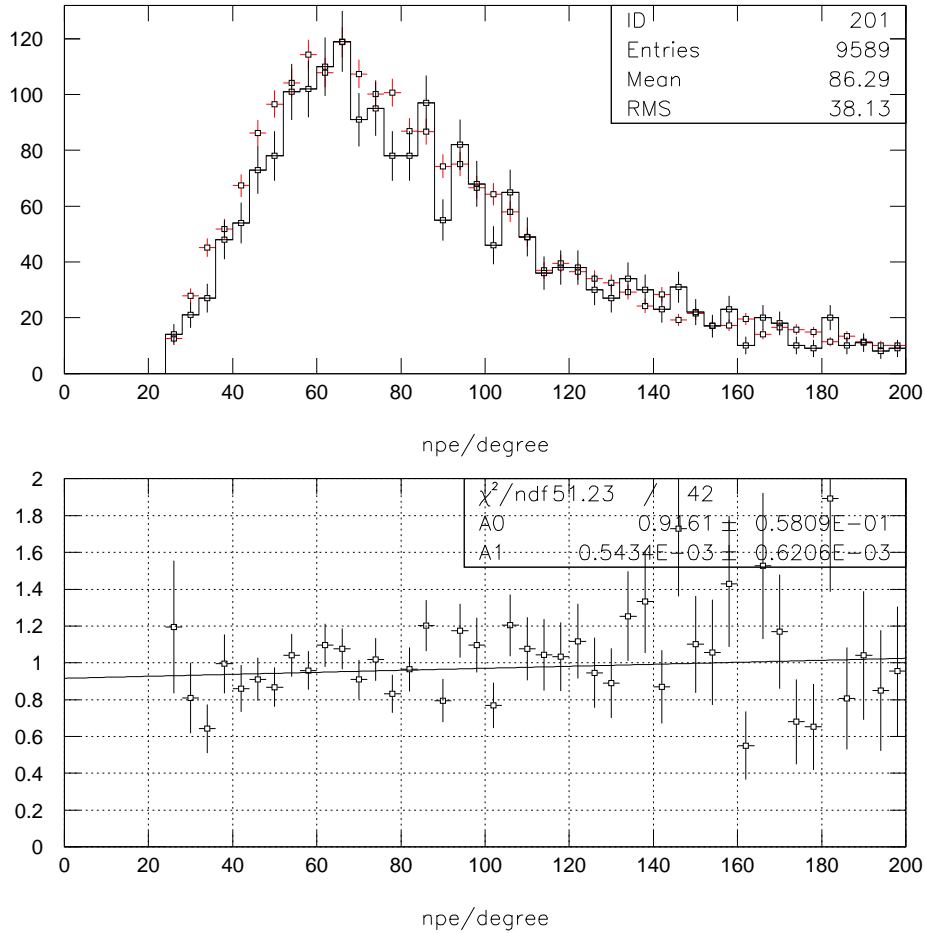


Fig. 7. Photoelectrons per degree of track

in the correction for unobserved energy in the shower is 5% [17].

Adding these uncertainties in quadrature yields a net systematic uncertainty on  $J(E)$ , averaged over energy, of 21%.

## 7 HiRes-I Analysis

In addition to the monocular data collected by the HiRes-II detector we have a considerable amount of monocular data collected by HiRes-I. In this section we describe the differences between the two detectors and their analyses, and in the next section present both monocular spectra.

In addition to the fact that HiRes-I has one ring of mirrors (rather than the

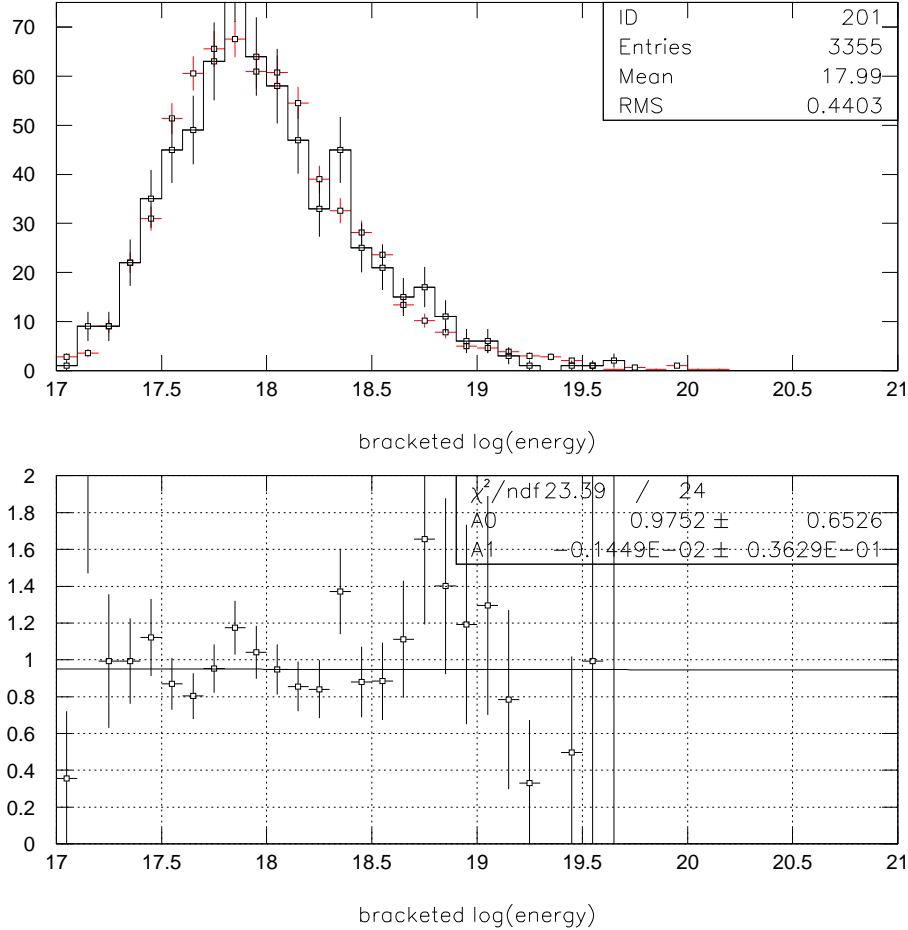


Fig. 8. Reconstructed Energy

two at HiRes-II) and sample and hold electronics (rather than flash ADC readout), the biggest difference is that we have data covering four years of running (rather than the six months quoted from HiRes-II), and the HiRes-I data has shorter tracks.

In reconstructing the geometry of tracks seen by the HiRes-I detector we wish to measure  $R_p$  and  $\psi$  from the curvature in the time plot (a HiRes-II time plot is displayed in the lower left quadrant of Figure 2). But the shorter tracks means the uncertainty in  $R_p$  and  $\psi$  are greater than we would wish for many events. To solve this problem we add to our fitting procedure a constraint based on the longitudinal energy deposition profile of the event (for a HiRes-II longitudinal profile plot see the lower right quadrant of Figure 2). From previous experiments using fluorescence detectors [15], and from the HiRes-II analysis reported here, we know that the Gaisser-Hillas formula in Equation 2 fits our events very well. While  $X_{max}$  varies from event to event and depends



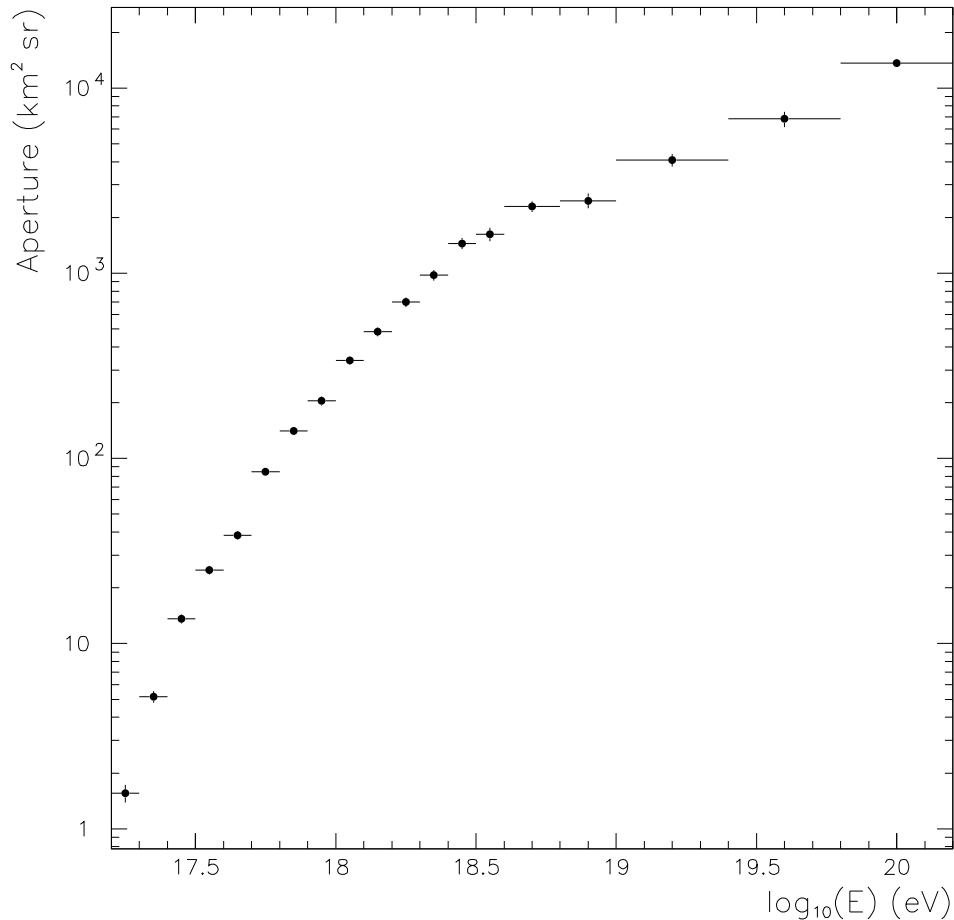


Fig. 9. Aperture of the HiRes-II detector used for this spectrum measurement.

logarithmically on the atomic weight of the nucleus and initial energy, the shape of the shower is largely independent of these, so effectively we use the fact that the shower width does not change with energy or composition to constrain the fit.

The profile-constrained geometry fit proceeds by first calculating a combined  $\chi^2$  for the time and profile fits. Each phototube on the track makes one contribution to the time fit and one to the profile fit. A map of  $\chi^2$  is made in six steps in  $x_{max}$  and 180 steps in  $\psi$ . The  $x_{max}$  values used are 685, 720, 755, 790, 825, and 960 gm cm<sup>-2</sup>. These values span the range of  $x_{max}$  values expected for our energy range. The  $\psi$  values range from 1 to 180 degrees. For each of the map points the fit is performed with the Gaisser-Hillas parameter  $x_0$  fixed to 40 gm cm<sup>-2</sup>. In the vicinity of the minimum of the  $\chi^2$  map a finer search is performed, which includes varying the orientation of the shower-detector plane within bounds of the fired photomultiplier tube apertures. To ensure

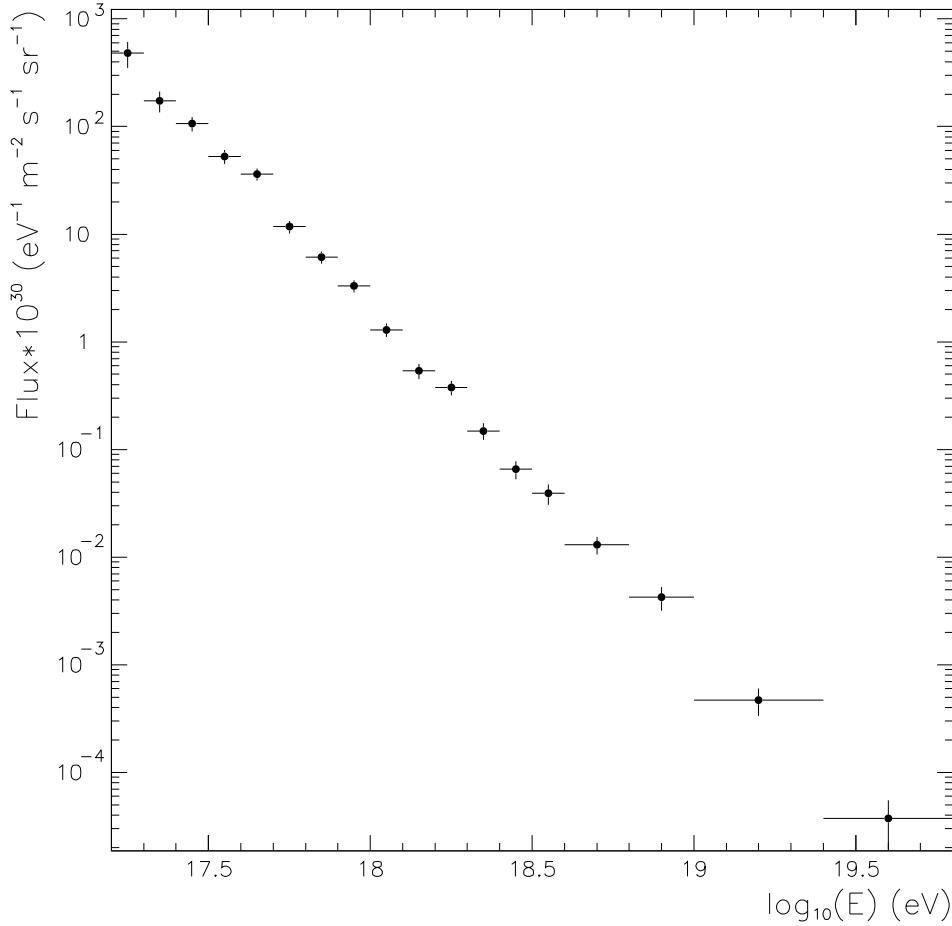


Fig. 10. Flux of UHE Cosmic Rays measured by the HiRes-II detector.

that the reconstruction process has been accurate we demand that:

- The Cerenkov light contribution to the observed flux be less than 20%,
- The tracklength be greater than 7.9 degrees,
- The depth of the first observed point be less than  $1200 \text{ gm cm}^{-2}$ ,
- The profile  $\chi^2/\text{d.o.f.}$  be less than 14,
- Angular speed  $< 3.4^\circ \mu\text{s}^{-1}$

In a Monte Carlo study of the profile-constrained geometry fit we find that the method works well, but introduces a small bias into the reconstructed energy. The bias is 15% at  $3 \times 10^{18}$  eV and falls to 5% at  $3 \times 10^{19}$  eV. Figure 12 shows the reconstructed energy divided by the Monte Carlo thrown energy at  $3 \times 10^{18}$  eV. The bias is evident from the fact that the peak does not occur at 1. Superimposed upon this plot is a similar plot determined from our stereo data. Here the stereo information was used to determine the geometry of the

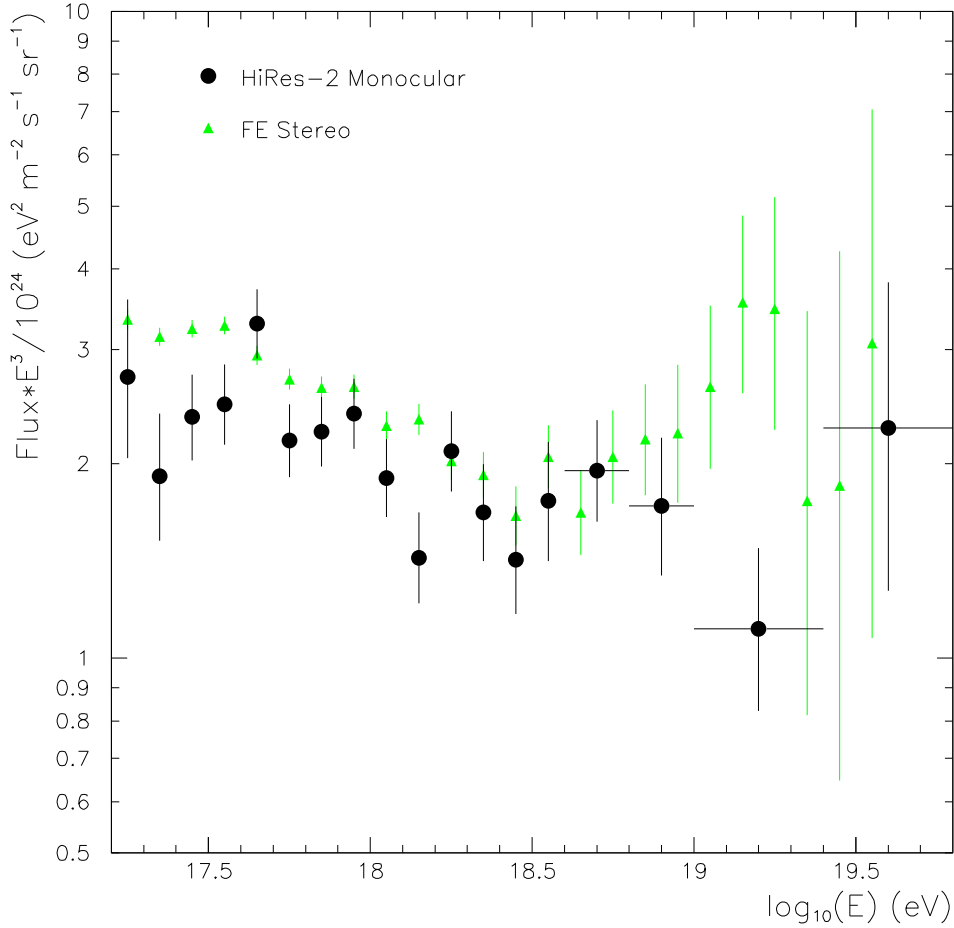


Fig. 11.  $E^3$  times the HiRes-II UHE Cosmic Ray Flux. The Fly’s Eye stereo spectrum is also shown.

event, and is like the Monte Carlo in that the stereo geometrical accuracy is much better than that of the HiRes-I mono reconstruction. The two curves agree very well. The shift was parameterized and a correction applied to the data.

Our Monte Carlo describes the HiRes-I data well. As an example, Figure 13 is a comparison between data and Monte Carlo of  $R_p$ , the impact parameter of showers, for events where  $18.4 < \log E(\text{eV}) < 18.6$ . The agreement is excellent.

Systematic uncertainties of the HiRes-I data are similar to those for HiRes-II. Changing the aerosol scale height by one standard deviation results in a change in the normalization of  $J(E)$  by  $(14 \pm 4)\%$  and introduces a slope of  $(-23 \pm 3)\%$  per decade of energy. The calibration uncertainty is 10%, the fluorescence yield uncertainty is 10%, and unobserved-energy correction is 5%. Adding uncertainties in quadrature yields a net systematic uncertainty

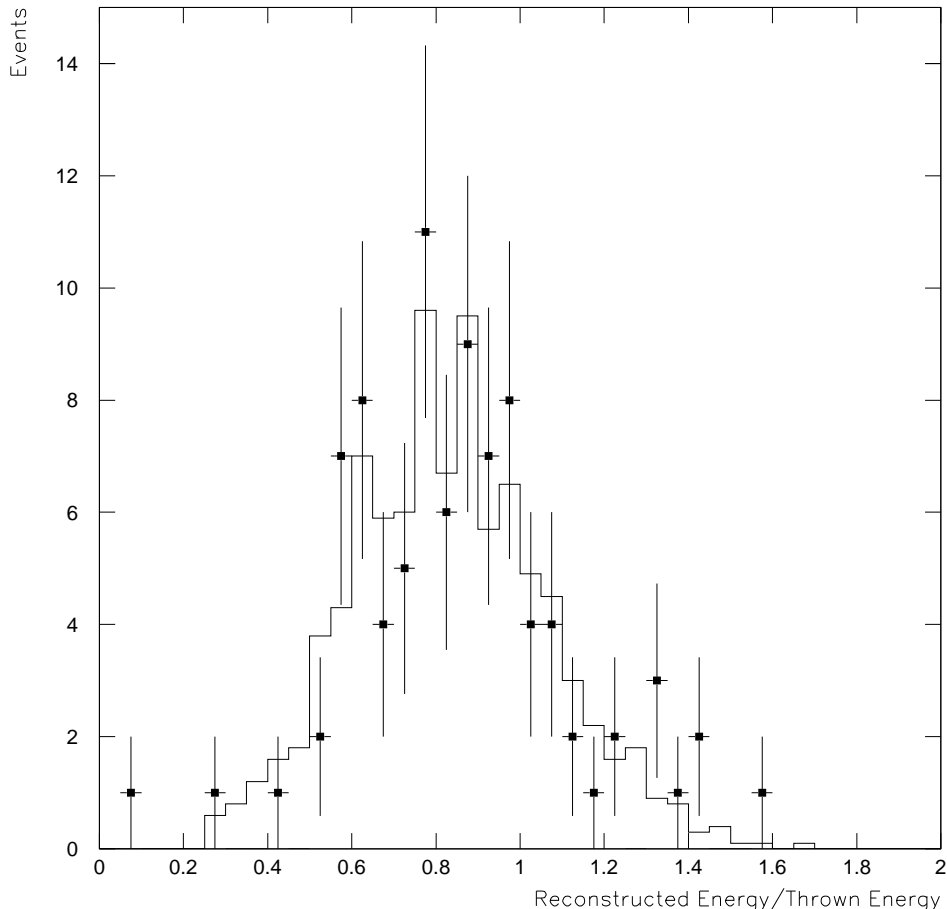


Fig. 12. Ratio of HiRes-I reconstructed energy to thrown energy. The histogram is for Monte Carlo events. The black points show stereo events from the data where the Monte Carlo thrown energy has been replaced with the energy calculated from the stereo geometric reconstruction.

on  $J(E)$ , averaged over energy, of 21%.

## 8 Discussion

In Figure 14, the monocular spectra from both the HiRes-I and HiRes-II detectors are shown [20]. In the energy range where both detectors' data have good statistical power the results agree with each other very well. The highest energy HiRes-I data point corresponds to one event reconstructed at  $1.84 \times 10^{20}$  eV. The latest (unpublished) results of the AGASA experiment are also shown in this figure [21]. Below about  $1 \times 10^{20}$  eV the AGASA results are consistently

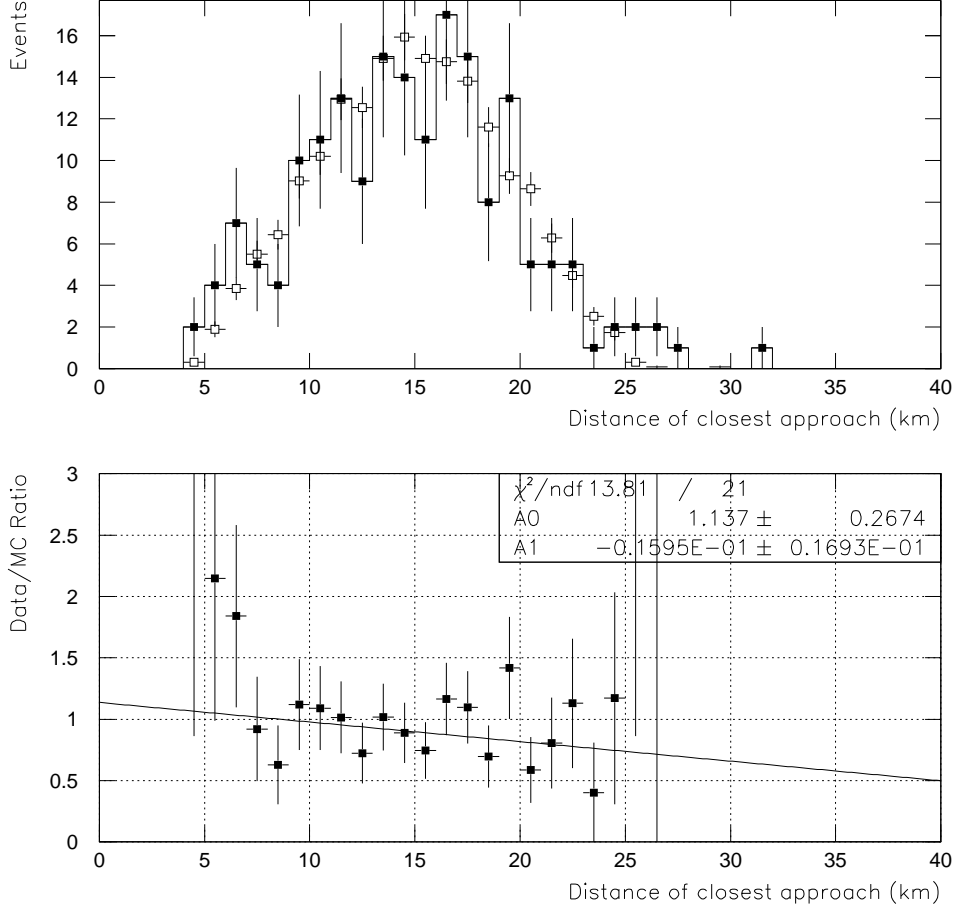


Fig. 13. Comparison between data and Monte Carlo for  $R_p$ , the impact parameter of showers, for events where  $18.4 < \log E(\text{eV}) < 18.6$

a factor of two higher than ours. Above this energy their data points diverge from the trend of our data.

Since the vertical axis in Figure 14 is  $E^3 \times J(E)$  a modest change in the energy scale would bring the experiments into considerably better agreement. For example lowering the AGASA energy scale by 20% would bring their points down by a factor of 2, move them to the left by 0.1 in  $\log(E)$ , and reduce the discrepancy between the two experiments. Such a change is within the systematic uncertainties of each experiment.

In the energy range,  $18.7 < \log E < 19.8$  the HiRes data is fit by an  $E^{-2.8}$  power law. The three highest-energy data points do not lie along an extension of that power law. Such an extension would predict that 19.1 events would occur above  $\log E = 19.8$  but only 5 were seen. The Poisson statistics proba-

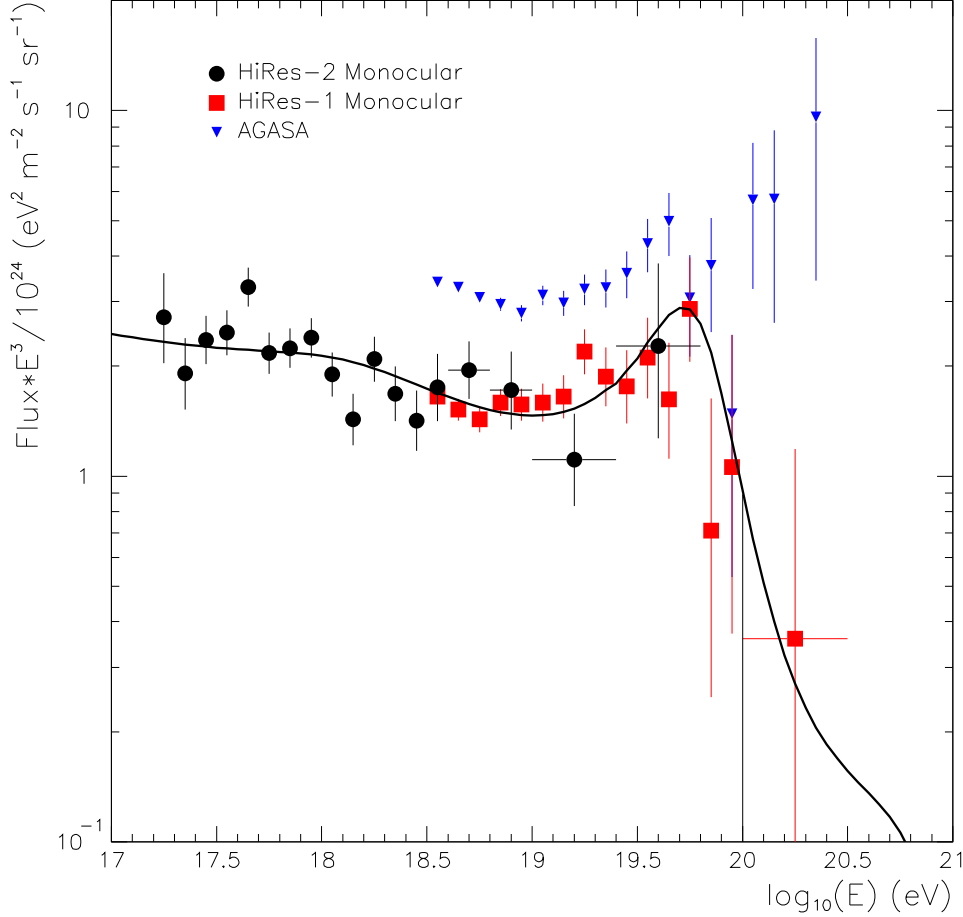


Fig. 14.  $E^3$  times the UHE Cosmic Ray Flux. Results from the HiRes-I and HiRes-II detectors, and the AGASA experiment are shown. Also shown is a fit to the data assuming a model, described in the text, of galactic and extragalactic sources.

bility of 5 or fewer events is  $1.4 \times 10^{-4}$ . But our data are consistent with the GZK cutoff. As an example of what one would expect we have fit the data to a model that consists of two sources for cosmic rays, galactic and extragalactic, which includes the GZK cutoff [22]. We use the extragalactic source model of Berezhinsky, Gazizov, and Grigorieva [23] which assumes that protons come from sources distributed uniformly across the universe, and lose energy by pion and  $e^+e^-$  production from the cosmic microwave background radiation, as well as from the expansion of the universe. Since the measured composition [4] is heavy at the lower end of our energy range, with the iron content decreasing linearly with  $\log E$ , we approximate the galactic component of cosmic rays as falling with an  $E^{-3}$  spectrum up to  $10^{17}$  eV, then decreasing as  $E^{-3} \times (19.5 - \log E)$  up to  $\log(E) = 19.5$ , and zero after. The model includes the experimental energy resolution, and an end to the extragalactic spectrum

at  $1 \times 10^{21}$  eV. The fitting parameters of the model are the normalization of the galactic events, and the power law index and normalization (at the source) of extragalactic cosmic rays. The fit is excellent with  $\chi^2$  of 45.7 for 34 degrees of freedom. In this model the peak at  $\log E$  of 19.8 is due to pion production pile-up, the ankle is made by losses due to  $e^+e^-$  production, and the second knee comes from  $e^+e^-$  production pile-up.

## 9 Conclusions

We have measured the flux of UHE cosmic rays with the FADC detector of the HiRes experiment. Use of flash ADC information allowed us to reduce systematic errors in reconstruction of events. We developed our Monte Carlo simulation programs to very accurately model the experiment, and calculated the exposure of the experiment in a way that takes into account the experimental resolution. The result reported here is in good agreement with the cosmic ray flux measurement made with the HiRes-I detector. The latter measurement is based on a statistically independent data set. The result reported here is also consistent with the flux measured by the Fly's Eye experiment using the stereo reconstruction technique. Above  $10^{20}$ eV our data is significantly different from that of the AGASA experiment. We have fit our data to a model incorporating both galactic and extragalactic sources of cosmic rays, which includes the GZK cutoff, and find good agreement.

## 10 Acknowledgements

This work is supported by US NSF grants PHY 9322298, PHY 9974537, PHY 9904048, PHY 0071069, by the DOE grant FG03-92ER40732, and by the Australian Research Council. We gratefully acknowledge the contributions from the technical staffs of our home institutions. The cooperation of Colonel E. Fischer, the US Army, and the Dugway Proving Ground staff is appreciated.

## References

- [1] R.J. Protheroe, Topics in Cosmic Ray Astrophysics (ed. M.A. DuVernois, Nova Science Publishing, NY, 1999) and astro-ph/9812055.
- [2] K. Greisen, Phys. Rev. Lett. **16**, 748 (1966); G. T. Zatsepin and V. A. Kuzmin, Pis'ma Zh. Eksp. Teor. Fiz. **4**, 114 (1966) [JETP Lett. **4**, 78 (1966)].

- [3] J. Linsley, Phys. Rev. Lett. **10**, 146 (1963) and Proc. 8th Int. Cosmic Ray Conf. **4**, 295 (1963).  
M.A. Lawrence, R.J.O. Reid, and A.A. Watson, J. Phys. G Nucl. Part. Phys. **17**, 733 (1991) and references therein.  
B.N. Afanasiev *et al.*, Proc. Tokyo Workshop on Techniques for the Study of Extremely High Energy Cosmic Rays (ed. M. Nagano, Inst. for Cosmic Ray Research, Univ. of Tokyo), 35 (1993).
- [4] D. J. Bird *et al.*, Phys. Rev. Lett. **71**, 3401 (1993) and Astrophys. J. **441**, 144 (1995). See also T. Abu-Zayyad *et al.*, Astrophys. J. **557**, 686 (2001).
- [5] M. Nagano *et al.*, J. Phys. G. **10**, 1295 (1984)
- [6] M. Ave *et al.*, astro-ph/0112253.
- [7] M.I. Pravdin *et al.*, Proc. 26th Int. Cosmic Ray Conf. (Salt Lake City), **3**, 292 (1999).
- [8] N. Sakaki for the AGASA Collaboratin, Proc. of 27th Int. Cosmic Ray Conf. (Hamburg) **1**, 333 (2001).
- [9] A.A. Watson, Proc. 25th Int. Cosmic Ray Conf. (Durban), **8**, 257 (1997) and references therein.
- [10] T. Abu-Zayyad *et al.*, Proc. 26th Int. Cosmic Ray Conf. (Salt Lake City), **5**, 349 (1999).
- [11] J. Boyer, B. Knapp, E. Mannel, and M. Seman, Nucl. Instr. Meth. **A482**, 457 (2002).
- [12] T. Abu-Zayyad *et al.*, to be submitted to NIM.
- [13] T. Abu-Zayyad *et al.*, in preparation.
- [14] T. K. Gaisser and A. M. Hillas, Proc. 15th Int. Cosmic Ray Conf. (Plovdiv), **8** 353, (1977).
- [15] T. Abu-Zayyad *et al.*, Astropart. Phys. **16**, 1 (2001).
- [16] F. Kakimoto *et al.*, Nucl. Instr. Meth. **A372**, 527 (1996). See also G. Davidson and R. O'Neil, J. Chem. Phys. **41**, 3946 (1964), and A. N. Bunner, Ph.D. Thesis, Cornell University, Ithaca, NY (1964).
- [17] C. Song *et al.*, Astropart. Phys. **14**, 7 (2000). See also J. Linsley, Proc. 18th ICRC, Bangalore, India, **12**, 144 (1983) and R.M. Baltrusaitis *et al.*, Proc. 19th ICRC, La Jolla, USA, **7**, 159 (1985).
- [18] Heck, D., Knapp, J., Capdevielle, J. N., Schatz, G., Thouw, T., Report FZKA 6019 (1998), Forschungszentrum Karlsruhe; [http://www-ik3.fzk.de/heck/corsika/physics\\_description/corsika\\_phys.html](http://www-ik3.fzk.de/heck/corsika/physics_description/corsika_phys.html)
- [19] N. N. Kalmykov, S. S. Ostapchenko, A. I. Pavlov, Nucl. Phys. B (Proc. Suppl.) **52B**, 17 (1997).



- [20] T. Abu-Zayyad *et al.*, submitted to Phys. Rev. Lett., astro-ph/0208243.
- [21] M. Teshima, private communication. This spectrum contains events seen at zenith angles less than  $45^\circ$ , and is lower than what was shown at the 27th International Cosmic Ray Conference.
- [22] See T. Abu-Zayyad *et al.*, in preparation.
- [23] V. Berezhinsky, A.Z. Gazizov, S.I Grigorieva, hep-ph/0204357.